Reports

Visualization of Turbulent Flame Fronts with Planar Laser-Induced Fluorescence

Abstract. *This report concerns the quantitative time-resolved visualization of reaction zones in laminar, transitional, and turbulent nonpremixed flames. Two-dimensional OH molecular concentrations were measured with planar laser-induced fluorescence excited by a sheet of light (formed from a single tunable ultraviolet laser pulse) and detected with a two-dimensional, image-intensified photodiode array camera. From the resulting data details of instantaneous flame front structures (including positions, shapes, and widths) were obtained.*

Many important processes such as turbulent combustion, atmospheric chemistry, chemical lasing, and chemical processing involve a complicated interplay between fluid mixing and chemical kinetics (*1*). Although the basic relations underlying these phenomena are fairly well established in nonreacting turbulent flows or reacting laminar flows, the understanding of reacting turbulent flows remains limited. However, the combination of numerical modeling and laser-based experimental measurements promises rapid advancement in this field.

Two approaches to the numerical modeling of chemically reacting turbulent flows have been developed. The Eulerian approach characterizes the turbulent fluctuations at any point in the flow in terms of probability density functions and takes only secondary account of the structure of mixing or reaction zones (*1–3*). The Lagrangian approach assumes that large-scale "coherent" vortex structures dominate turbulent mixing and models the formation, development, and motion of these structures (*4–6*).

Structural aspects of flames and turbulent mixing have been studied by simultaneous, multiple-point laser measurements based on Mie (*7–9*), Raman (*10*), and Rayleigh (*11, 12*) scattering as well as one-dimensional imaging of fluorescence (*13*). In the work reported here we used two-dimensional imaging of OH laser-induced fluorescence (*14–17*), which has several advantages over the other methods. Fluorescence is much more sensitive than Rayleigh or Raman scattering and is capable of measuring OH concentrations of parts per million in flames at atmospheric pressure. Moreover, the fluorescence signals originate only from regions with large OH concentrations, which, in nonpremixed flames, occur primarily in the reaction zone. Thus OH fluorescence is an excellent indicator of reaction zone location and shape.

Laser-induced fluorescence is a resonance process that occurs when the frequency of a laser corresponds to an allowed electronic transition of a molecular species present in the laser beam. After being excited into an upper electronic state by absorption, a molecule returns to the ground electronic level either by spontaneously emitting a photon (fluorescence) or by transferring energy to other molecules through collisions (quenching). In our experiment the laser beam is expanded into a sheet and the induced fluorescence is detected with a multiple-element photodiode array. The resulting digital images can be related to the molecular species concentration in the plane of the laser beam.

For a spectrally broad laser source with pulse energy per unit area E and spectral width $\Delta\nu$, the number of photons n arriving from a given collection volume is

$$n = \eta\,(E/\Delta\nu)\,SFN \qquad (1)$$

where η is a function of the optical system, S is a function of the transition and the electronic quenching rate, N is the species number density in the collection volume, and F is the fractional population of molecules in the initial absorbing energy level. We wish to relate N to n in such a way that the effects of flow field variations are minimized. Thus our measurements were carried out at constant pressure and the molecular transition was chosen to minimize the temperature dependence of SF. The remaining parameters, η, E, and $\Delta\nu$, are independent of the flow field. Preliminary calculations indicate that the compositional variation of the quenching rate is small for the flames investigated. Absolute levels can be obtained by separate determination of the absolute molecular concentration at a point in the flow, using optical absorption or saturated laser-induced OH fluorescence (*18*).

The experimental arrangement is shown schematically in Fig. 1. A frequency-doubled, Molectron Nd:YAG–pumped dye laser (MY34/DL18) was tuned to the Q_1 (*6*) line of the $A^2\Sigma^+$ ($v = 0$) $\leftarrow$ $X^2\Pi$ ($v = 0$) band of OH. The ultraviolet laser pulse energy was 1 mJ with a duration of ~ 7 nsec. The beam was expanded into a sheet (~ 40 mm wide and 400 μm thick) by use of two fused silica cylindrical lenses, then deflected vertically through Suprasil windows in the combustor. A simple fused silica lens (focal length, 7.5 cm) imaged the fluorescence onto the front of an ITT dual-microchannel-plate image intensifier tube that provided nearly quantum-limited sensitivity. A fiber-optic bundle coupled the image intensifier tube to a 100 by 100 photodiode array (6 by 6 mm active area) that was part of a Reticon MC520/RS520 camera system. A Data Translation DT2782 analog-to-digital converter interfaced with an LSI 11/23

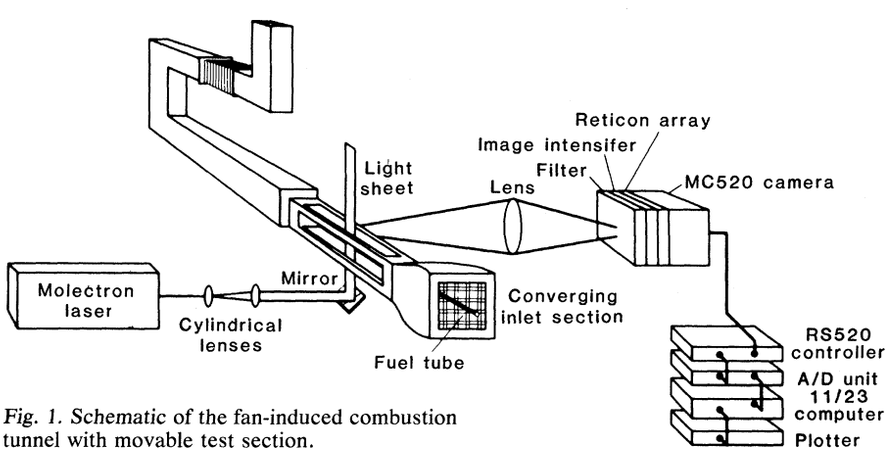

Fig. 1. Schematic of the fan-induced combustion tunnel with movable test section.

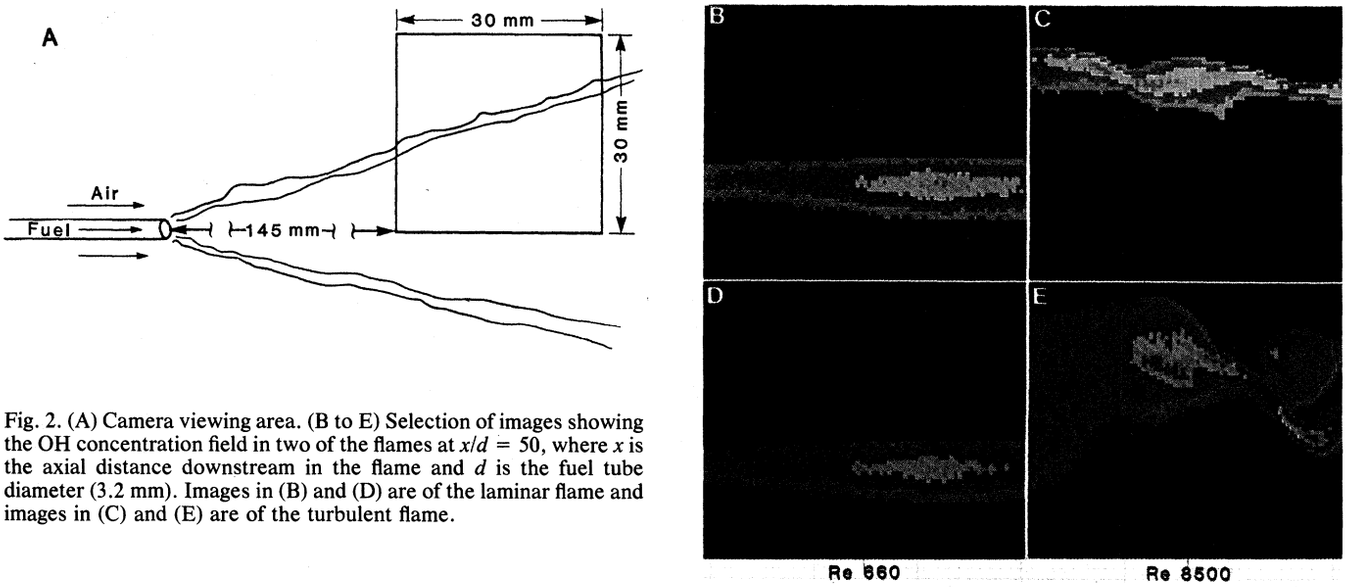

Fig. 2. (A) Camera viewing area. (B to E) Selection of images showing the OH concentration field in two of the flames at $x/d = 50$, where x is the axial distance downstream in the flame and d is the fuel tube diameter (3.2 mm). Images in (B) and (D) are of the laminar flame and images in (C) and (E) are of the turbulent flame.

computer digitized the output of the photodiode array. The resulting digital images were stored on floppy disks. Because the laser irradiance was not uniform, its distribution was measured and used to normalize the fluorescence data. The fractional absorption of the laser beam in the flame was estimated to be negligible, and the polarization of the laser was arranged to minimize Rayleigh scattering.

Nonpremixed jet flames (laminar, transitional, and turbulent) produced in the fan-induced combustion tunnel shown in Fig. 1 (*19–21*) were investigated. The laminar flame, characterized by its nominal cold flow H_2 Reynolds number (Re) of 660, had average initial H_2 and air velocities of 22.0 and 7.5 m/sec, respectively. The transitional flame (Re = 1600) had initial H_2 and air velocities of 54.0 and 9.8 m/sec, while the turbulent flame (Re = 8500) had H_2 and air velocities of 285 and 12.5 m/sec, respectively. The last two flames had been characterized previously by pulsed vibrational Raman point measurements of temperature and major species concentrations (*19, 21*) and by theoretical modeling studies (*20*).

Examples of OH images in the laminar and turbulent flames are shown in Figs. 2 and 3. The camera viewed an area of 3.0 by 3.0 cm and was adjusted so that the bottom edge of each image corresponded with the center line of the flame (Fig. 2A). Thus each element of the 100 by 100 array detected OH fluorescence from a sample volume of 0.3 by 0.3 by 0.4 mm. The maximum OH levels (shown in red) correspond to approximately 6×10^{16} molecules per cubic centimeter [based on the maximum OH concentrations measured with single-pulse laser saturated fluorescence (*18*)]. Eight levels of OH concentration are shown in Figs. 2 and 3, with black indicating an OH level less than one-tenth of the maximum in each frame.

The results show that laminar flames have reaction zone structures with little shot-to-shot variation in width and position (Fig. 2, B and D). Reaction zone widths (defined as twice the minimum distance for the measured OH concentration to decrease to one-tenth of its maximum value) measured in the laminar flame from 20 images (including those in Fig. 2) gave a most probable instantaneous reaction zone width of 5 mm, with a range of 3.6 to 5.7 mm. In contrast, the turbulent flame images (Fig. 2, C and E) indicate dramatic shot-to-shot changes in reaction zone width, position, and shape. Most of the images at this flame position had thin filament-like reaction zone shapes (Fig. 2C), but

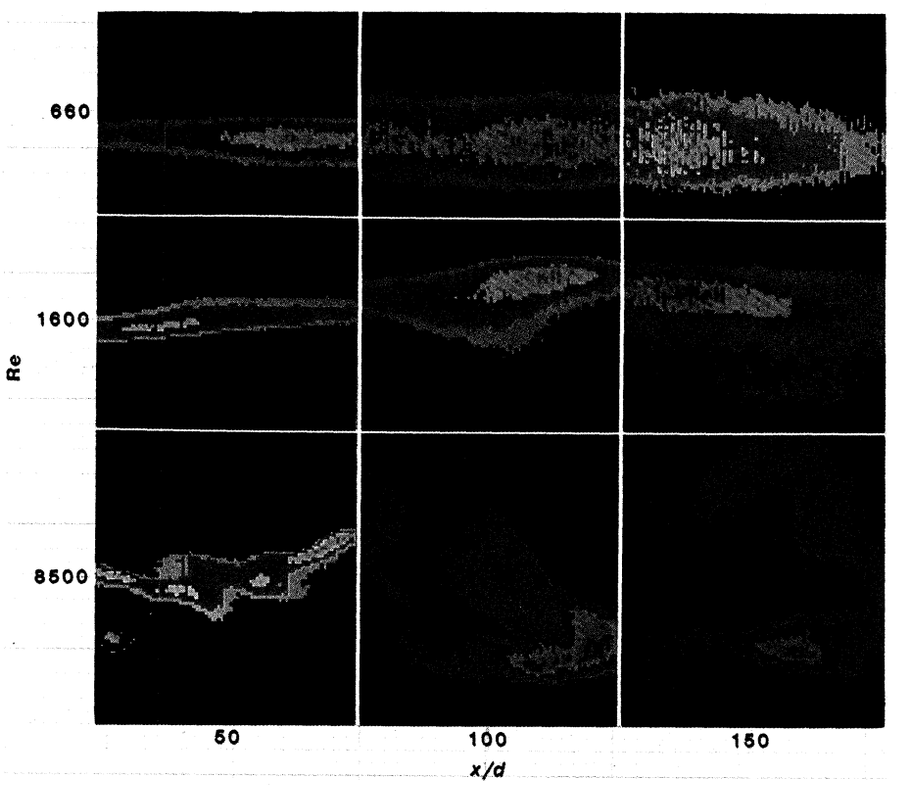

Fig. 3. Selection of images showing the OH concentration field in each of the three flames at each of the three locations investigated.

some broader vortex-like images (Fig. 2E) were observed. Forty images in the turbulent flame at $x/d = 50$ gave a most probable width of 2.1 mm with a broad range from 1.2 to 9.6 mm. The most probable width is smaller in the turbulent than in the laminar flame because of flame stretching due to increased shear. The wide range of measured turbulent flame zone widths may also be due to the reaction sheet not being perpendicular to the image plane or to overlapping of several different reaction zone sheets.

Figure 3 shows representative images from each of the flames at each of the positions investigated. The turbulent reaction zones observed at $x/d = 100$ and 150 differ qualitatively from the laminar, transitional, and even the $x/d = 50$ turbulent reaction zones; pockets appear that are not attached (at least in the imaged plane) to the rest of the reaction zone (see cover). In addition, the reaction zone sometimes does not extend continuously across the image, perhaps indicating breakup of the flame sheet.

The results reported here are qualitatively different from instantaneous flame fronts previously measured in premixed turbulent flames (*11*), where the instantaneous flame thicknesses were the same as the laminar premixed flame thicknesses (0.7 mm) and were independent of flame positions in accord with a "wrinkled laminar flame" model. Our measurements of nonpremixed turbulent flames indicate that (i) instantaneous flame thicknesses are considerably narrower than in laminar nonpremixed flames, (ii) flame thickness increases with downstream distance, and (iii) in some cases the flame sheet is apparently discontinuous.

The complex reaction zone structures that have been observed are in many ways similar to mixing zone structures in turbulent nonpremixed flames observed in Mie scattering studies (*9*). Such observations may help shed light on the importance of reaction zone and large-scale structures in understanding turbulent combustion and other reacting flow systems.

GEORGE KYCHAKOFF
ROBERT D. HOWE
RONALD K. HANSON
Department of Mechanical Engineering, Stanford University, Stanford, California 94305
MICHAEL C. DRAKE
ROBERT W. PITZ
MARSHALL LAPP*
C. MURRAY PENNEY
General Electric Research and Development Center, Schenectady, New York 12301

References and Notes

1. P. A. Libby and F. A. Williams, Eds., *Turbulent Reacting Flows* (Springer-Verlag, New York, 1980).
2. W. Kollmann, Ed., *Prediction Methods for Turbulent Flows* (McGraw-Hill, New York, 1980).
3. R. W. Bilger, *Combust. Flame* **26**, 115 (1976).
4. D. B. Spalding, *Proceedings of the 17th International Symposium on Combustion* (Combustion Institute, Pittsburgh, 1978), p. 431.
5. A. F. Ghoniem, A. J. Chorin, A. K. Oppenheim, *Philos. Trans. R. Soc. London Ser. A* **304**, 303 (1982).
6. A. K. Oppenheim and A. F. Ghoniem, *AIAA Pap. 83-0470* (1983).
7. M. B. Long, B. T. Chu, R. K. Chang, *AIAA J.* **19**, 1151 (1981).
8. M. B. Long and B. T. Chu, *ibid.*, p. 1158.
9. A. J. R. Lysaght, R. W. Bilger, J. H. Kent, *Combust. Flame* **46**, 105 (1982).
10. M. B. Long, D. Fourgette, M. C. Escoda, C. Layne, *Opt. Lett.* **8**, 244 (1983).
11. S. Rajan, J. R. Smith, G. D. Rambach, *West. States Sect. Combust. Inst. Pap. 82-88* (1982).
12. M. C. Escoda and M. B. Long, *AIAA J.* **21**, 81 (1983).
13. M. Alden, H. Edner, G. Holmsted, S. Svanberg, T. Hogberg, *Appl. Opt.* **21**, 1236 (1982).
14. M. J. Dyer and D. R. Crosley, *Opt. Lett.* **7**, 382 (1982).
15. G. Kychakoff, R. D. Howe, R. K. Hanson, J. C. McDaniel, *Appl. Opt.* **21**, 3225 (1982).
16. G. Kychakoff, K. Knapp, R. D. Howe, R. K. Hanson, *AIAA J.* **22**, 153 (1984).
17. G. Kychakoff, R. D. Howe, R. K. Hanson, *Appl. Opt.*, in press.
18. R. P. Lucht, D. W. Sweeney, N. M. Laurendeau, M. C. Drake, M. Lapp, R. Pitz, *Opt. Lett.*, in press.
19. M. C. Drake, M. Lapp, C. M. Penney, S. Warshaw, B. W. Gerhold, *Proceedings of the 18th International Symposium on Combustion* (Combustion Institute, Pittsburgh, 1981), p. 1521.
20. M. C. Drake, R. W. Bilger, S. H. Starner, *Proceedings of the 19th International Symposium on Combustion* (Combustion Institute, Pittsburgh, 1982), p. 459.
21. M. C. Drake, M. Lapp, C. M. Penney, S. Warshaw, B. W. Gerhold, *AIAA Pap. 81-0103* (1981).
22. We are grateful to the Office of Naval Research (contract N00014-80-C-0882, NR-094-405) for supporting major portions of this work and to the Air Force Office of Scientific Research (contract F49620-80C-0091) for additional support of the Stanford group. We also acknowledge valuable interactions with F. Gouldin of Cornell University that helped to define the direction of this research and significant contributions to the experimental program by F. Haller and F. Haskell.
* Present address: Sandia National Laboratories, Livermore, Calif. 94550.

15 March 1983; accepted 25 August 1983

Turbidity Currents: Monitoring Their Occurrence and Movement with a Three-Dimensional Sensor Network

Abstract. *Detailed field data on the occurrence, flow pattern, and internal dynamics of both surge and continuous turbidity currents have been obtained with a three-dimensional array of optical and thermal sensors. The array, operated in a glacial lake in southeastern British Columbia, collected detailed information on the character of surge events with velocities reaching 110 centimeters per second and continuous underflows exceeding 90 centimeters per second. The findings (i) indicate that such currents are frequent events, occurring with density differences between the incoming stream water and the lake water as low as 0.19 kilogram per cubic meter of water; (ii) document the differences in the initiation and internal characteristics of the continuous and surge events; and (iii) support the concept of erosion by turbidity currents.*

The general laws describing the movement of turbidity currents have been the subject of considerable laboratory and theoretical study by geologists, engineers, and fluid dynamicists (*1*). Yet the collection of field data on such phenomena in differing environments has been limited to measurements over relatively short time spans and at only a few measurement points. As Normark (*2*) and others have pointed out, this lack of detailed field observations has left present theory with only limited empirical support. In an effort to provide more detailed field data, a three-dimensional array of optical and thermal sensors and a smaller system of current meters were installed and operated in a glacial lake in southeastern British Columbia during the summers of 1977 and 1978. The network provided both a continuous record of the occurrence of underflow events and surge events and data on the internal characteristics of the flows. To my knowledge, this work constitutes the first use of a three-dimensional network in the study of turbidity currents.

A glacial lake provides excellent opportunities for measuring turbidity currents because of the often high and rapidly fluctuating discharge and sediment loads associated with most glacial meltwater systems and because of the diminished thermal, biological, and pollutant effects. The particular lake selected for monitoring is in the central Purcell range at 51°N, 116°W. Its relatively simple hydrologic setting, with only one main glacially fed stream entering it, gently varying lake-bottom topography, shallow mean depth of 5 m, and small size of less than 0.5 km^2 made it an ideal natural laboratory for the study of turbidity currents (Fig. 1).

The primary instrument network was designed to monitor the passage of underflow currents down the foreslope and into the lake. It consisted of 27 sensor packages organized in a 3 by 3 by 3 array (Fig. 1). Each package includes a tem-